Cells & Development 179 (2024) 203935

Contents lists available at ScienceDirect

Cells & Development

journal homepage: www.journals.elsevier.com/cells-and-development

The pluripotency state of human embryonic stem cells derived from single blastomeres of eight-cell embryos

Ot Massafret [a,b], Montserrat Barragán [c], Lucía Álvarez-González [a,d], Begoña Aran [e], Beatriz Martín-Mur [f], Anna Esteve-Codina [f,g], Aurora Ruiz-Herrera [a,d], Elena Ibáñez [a,*], Josep Santaló [a]

[a] Genome Integrity and Reproductive Biology Group, Departament de Biologia Cel·lular, Fisiologia i Immunologia, Facultat de Biociències, Universitat Autònoma de Barcelona, 08193 Bellaterra, Spain
[b] Bioengineering in Reproductive Health, Institute for Bioengineering of Catalonia (IBEC), The Barcelona Institute of Science and Technology (BIST), 08028 Barcelona, Spain
[c] Basic Research Laboratory, Eugin Group, Parc Científic de Barcelona, 08028 Barcelona, Spain
[d] Genome Integrity and Instability Group, Institut de Biotecnologia i Biomedicina, Universitat Autònoma de Barcelona, 08193 Bellaterra, Spain
[e] Stem Cell Bank, Regenerative Medicine Program, Institut d'Investigació Biomèdica de Bellvitge (IDIBELL), 08908 L'Hospitalet de Llobregat, Spain
[f] CNAG-CRG, Centre for Genomic Regulation, Barcelona Institute of Science and Technology, 08028 Barcelona, Spain.
[g] Universitat Pompeu Fabra (UPF), Barcelona, Spain

ARTICLE INFO

Keywords:
hESC
Derivation
Blastomeres
Naïve
Primed
Pluripotency

ABSTRACT

Human embryonic stem cells (hESCs) derived from blastocyst stage embryos present a primed state of pluripotency, whereas mouse ESCs (mESCs) display naïve pluripotency. Their unique characteristics make naïve hESCs more suitable for particular applications in biomedical research. This work aimed to derive hESCs from single blastomeres and determine their pluripotency state, which is currently unclear. We derived hESC lines from single blastomeres of 8-cell embryos and from whole blastocysts, and analysed several naïve pluripotency indicators, their transcriptomic profile and their trilineage differentiation potential. No significant differences were observed between blastomere-derived hESCs (bm-hESCs) and blastocyst-derived hESCs (bc-hESCs) for most naïve pluripotency indicators, including TFE3 localization, mitochondrial activity, and global DNA methylation and hydroxymethylation, nor for their trilineage differentiation potential. Nevertheless, bm-hESCs showed an increased single-cell clonogenicity and a higher expression of naïve pluripotency markers at early passages than bc-hESCs. Furthermore, RNA-seq revealed that bc-hESCs overexpressed a set of genes related to the post-implantational epiblast. Altogether, these results suggest that bm-hESCs, although displaying primed pluripotency, would be slightly closer to the naïve end of the pluripotency continuum than bc-hESCs.

1. Introduction

Embryonic stem cells (ESCs) can exist in at least two different states of pluripotency: naïve and primed (Nichols and Smith, 2009). Traditional methods to derive human ESCs (hESCs) produce primed lines (Nichols and Smith, 2009), whereas mouse ESCs (mESCs) typically display naïve pluripotency. The mechanism by which naïve pluripotent cells of the inner cell mass transit to the primed pluripotency of hESCs established in vitro is not fully understood. O'Leary et al. (O'Leary et al., 2012) described the formation of a transient epiblast-like structure a few days after plating human blastocysts, which they termed the post-inner cell mass intermediate (PICMI). Its formation was found to be a necessary step for the generation of a new hESC line (O'Leary et al., 2012) and was proposed to be a turning point between the naïve pluripotency of the pre-implantation epiblast and the primed pluripotency of hESCs (van der Jeught et al., 2015; Warrier et al., 2018).

Naïve stem cells are preferred over primed stem cells for some particular applications, mainly for in vitro modelling of embryo development. The extraembryonic lineage differentiation potential of naïve hESCs allows a better understanding of trophectoderm development (Zhou et al., 2023). Additionally, thanks to their increased potential, naïve hESCs can be used to generate blastoids, in vitro 3-D structures

* Corresponding author.
E-mail address: elena.ibanez@uab.cat (E. Ibáñez).

https://doi.org/10.1016/j.cdev.2024.203935
Received 26 April 2024; Received in revised form 17 June 2024; Accepted 20 June 2024
Available online 22 June 2024

that replicate the embryo at the blastocyst stage (Yu et al., 2021a) and, more recently, two groups have used naïve hESCs to generate structures that model the post-implantation human embryo until as late as day 14 (Oldak et al., 2023; Weatherbee et al., 2023).

During the last decade, several groups have developed protocols based on the 2i condition (a combination of GSK3β and MEK inhibitors) to obtain hESCs in a naïve pluripotency state resembling that of mESCs (Chen et al., 2015; Chan et al., 2013; Duggal et al., 2015; Gafni et al., 2013; Guo et al., 2016, 2017; Hanna et al., 2010; Hu et al., 2020; Qin et al., 2016; Takashima et al., 2014; Theunissen et al., 2014; Valamehr et al., 2014; Ware et al., 2014). Some of these groups achieved direct derivation of a few naïve hESC lines from preimplantation embryos (Gafni et al., 2013; Guo et al., 2016; Theunissen et al., 2014; Ware et al., 2014), although efficiency rates, when specified, were very low (e.g. 1 line out of 128 embryos in Ware et al., 2014 (Ware et al., 2014)).

Even though it is well known that culture conditions influence the pluripotency state of hESCs, the potential effect of the developmental stage of the preimplantation embryo from which the hESCs are derived is unclear. hESCs were first derived from blastocysts (Thomson, 1998), but derivation from single blastomeres of cleavage-stage embryos has also been achieved by several groups (Chung et al., 2008; Geens et al., 2009; Ilic et al., 2009; Klimanskaya et al., 2006; Taei et al., 2013; Yang et al., 2013). Comparison of the transcriptome of blastomere-derived hESCs (bm-hESCs) and blastocyst-derived hESCs (bc-hESCs) has provided contradictory results. Some authors reported that bm-hESCs and bc-hESCs share similar transcription profiles (Giritharan et al., 2011; Galan et al., 2013), whereas another study found significant differences in their transcriptomes (Zdravkovic et al., 2015). The latter study also reported that bm-hESCs had an increased capacity to differentiate into trophectodermal lineages, which could be indicative of a more naïve pluripotency state. In line with this study, another work observed a shift from random to skewed X-chromosome inactivation along with culture passages in bm-hESCs (Geens et al., 2016). This suggested that bm-hESCs could present a more naïve pluripotency state, at least at early passages, although the naïve characteristics would be gradually lost during prolonged culture.

To test this hypothesis, we derived new hESC lines from single blastomeres of 8-cell stage embryos, as well as from whole blastocysts, using the same conditions. We analysed a wide array of naïve pluripotency indicators, their transcriptomic profile, and their ability to differentiate into cells of the three primary germ layers, to assess the influence of the developmental stage of the donor embryo on the pluripotency state of hESCs at early culture passages.

2. Materials and methods

2.1. Embryo thawing and culture

A total of 264 human embryos from 52 couples, donated at different reproduction centres in Barcelona, were used: 10 embryos were cryopreserved at the 2PN stage, 129 at D2, 61 at D3, and 64 at D5 or D6.

Vitrified embryos were thawed using the Irvine Vit Kit-Thaw (Irvine Scientific), following manufacturer's instructions. Ultra-rapid frozen embryos were thawed using the Global® Blastocyst Fast Freeze® Thawing Kit (LifeGlobal), following manufacturer's instructions. Slow-frozen embryos were thawed as follows: the straw was removed from liquid N2 and held for 40 s at room temperature (RT) and for 40 s in a water bath at 30 °C. After that, the content of the straw was emptied directly on a petri dish and incubated for 15 min at RT. The embryos were then transferred to a drop of KSOM-H medium (prepared in-house) and incubated for 15 min at 37 °C.

Embryos were cultured at 37 °C, 5 % CO_2 in drops of Global Total medium (LifeGlobal) covered with mineral oil until they reached the required developmental stage. GSK3β inhibitor CHIR99021 (CH; Axon Medchem) and ROCK inhibitor Y-27632 (Y; Stemcell Technologies) were added to the culture media when indicated.

2.2. Feeder cells culture and inactivation

Human Foreskin Fibroblasts (HFF-1, ATCC®SCRC-1041™) were used as feeder cells. HFFs were cultured for expansion in DMEM (Gibco) containing 10 % Foetal Bovine Serum (FBS; Gibco). Cells were inactivated by incubation with 10 μg/ml mitomycin C (Fisher Scientific) for 3 h. Inactivated HFFs (iHFFs) were then seeded on either 4 well plates for the derivation of hESCs from whole blastocysts or in 50 μl drops on 60 mm petri dishes for the derivation of hESCs from single blastomeres.

2.3. Derivation and culture of hESCs

Derivation was performed from whole blastocysts and from single blastomeres isolated from 8-cell embryos using a protocol based on Taei et al. (Taei et al., 2013) Exceptionally, a small number of embryos were biopsied at 6, 7, 9 or 10-cell stages, in all cases before showing any signs of compaction. Blastocysts at D5 or D6 of development were dezoned with Tyrode's Acidic Solution (Sigma), seeded onto a monolayer of iHFFs, and monitored daily from day 3 onwards. Single blastomeres were biopsied from 6- to 10-cell embryos, individually seeded onto a monolayer of iHFFs and monitored every day from day 3 onwards to check for cell division. All blastomeres from each embryo were biopsied to reduce the number of embryos used.

The medium for hESC derivation consisted of KO-DMEM (Gibco) containing 20 % Knockout Serum Replacement (KSR; Thermo Fisher), 2 mM L-glutamine (BioWest), 1× MEM-non-essential amino acids (Gibco), 50 mM 2-mercaptoethanol (Gibco), 1× ITS-X (Gibco), 10000 U/ml penicillin - 10 mg/ml streptomycin (Gibco), and 4 ng/ml human Fibroblast Growth Factor-basic (bFGF; Gibco). When indicated, 1 mM ROCK inhibitor Y and 3 mM GSK3β inhibitor CH were added to the medium. All culture procedures were performed in a humidified incubator at 37 °C and 5 % CO_2 in air.

Blastocyst and blastomere outgrowths were passaged mechanically on day 6–7 and 10–12, respectively. In both cases, if a PICMI was observed, it was mechanically isolated and passaged individually. If a PICMI was not observed, the entire outgrowth was passaged. The medium was changed every other day and hESC colonies were passaged either mechanically or enzymatically as small clumps with trypsin-EDTA (BioWest) every 6–7 days.

2.4. Conversion of a pre-existing primed hESC line

A naïve hESC line was generated from an established blastocyst-derived hESC line (ES[10] line, 46, XX, obtained from the Spanish National Stem Cell Bank and registered in the human Pluripotent Stem Cell Registry as ESe025-A) using a modification of the protocol described by Ware and colleagues (Ware et al., 2014). Briefly, hESCs were first cultured for two passages in hESC medium supplemented with 0.1 mM sodium butyrate (Sigma) and 50 nM SAHA (Santa Cruz), and then passaged as single cells and maintained in 2iF medium at 37 °C and 5 % CO_2 in air. This naïve-converted hESC line was maintained for >25 passages in 2iF medium.

2.5. Characterization of hESC lines

2.5.1. Immunostaining for intracellular markers

Putative newly generated hESC lines were characterized by immunofluorescence of pluripotency markers OCT4 and SOX2. Differentiation markers alpha-fetoprotein (AFP) for endoderm, alpha smooth muscle actin (SMA) for mesoderm and class III beta-tubulin (TUJ1) for ectoderm were also analysed after inducing spontaneous differentiation by culturing colonies in DMEM supplemented with 10 % FBS without feeder cells for 7–10 days.

hESC colonies grown on coverslips were fixed with 4 % paraformaldehyde (PFA) for 20 min at RT and then washed three times with 1× PBS for 5 min. After that, the cells were permeabilised and blocked in

a PBS solution containing 0.2 % sodium azide (Sigma), 0.5 % Triton X-100 (Sigma), and 3 % goat serum (BioWest) for 30 min at 37 °C. The cells were then incubated with the primary antibody overnight in a wet chamber at 4 °C. The next day, cells were washed three times with 1× PBS for 5 min each before adding the corresponding secondary antibody and incubating for 2 h at RT in the dark. All the antibodies were diluted in a PBS-based solution containing 0.2 % sodium azide, 0.1 % Triton X-100, and 3 % goat serum.

After that, 10 µg/ml Hoechst 33258 (Molecular Probes – Invitrogen) diluted in Vectashield (Vector Laboratories) was added as a nuclear counterstain and coverslips were mounted on slides. The preparations were kept at −20 °C until they were analysed using an epifluorescence microscope (Olympus BX61). Images were obtained using Cytovision software (Applied Imaging, Inc.).

Primary antibodies used were mouse monoclonal anti-OCT4 (Santa Cruz, sc-5279, dilution 1:50), rabbit polyclonal anti-SOX2 (Merck, AB5603, dilution 1:200), mouse monoclonal anti-AFP (R&D Systems, MAB1368, dilution 1:200), mouse monoclonal anti-SMA (Sigma, A5228, dilution 1:200), mouse monoclonal anti-TUJ1 (Covance, MMS-435P, dilution 1:500), and rabbit polyclonal anti-H3K27me3 (Merck, 07–449, dilution 1:500).

Secondary antibodies used were chicken anti-mouse IgG Alexa Fluor 488 (Molecular Probes, A-21200, dilution 1:500) and goat anti-rabbit IgG Alexa Fluor 594 (Molecular Probes, A-11037, dilution 1:500).

2.5.2. Immunostaining for cell surface marker SSEA3

To detect the cell surface SSEA3 pluripotency marker, hESCs were fixed with 4 % PFA, blocked, and permeabilized with TBS containing 0.5 % Triton X-100 and 6 % donkey serum (Chemicon) (Martí et al., 2013). Cells were incubated overnight with rat anti-SSEA3 primary antibody (Developmental Studies Hybridoma Bank, MC-631, dilution 1:1) diluted in TBS containing 0.1 % Triton X-100 and 6 % donkey serum. Next, cells were incubated with goat anti-rat IgM Cy3 secondary antibody (Jackson ImmunoResearch, 112–165-020, dilution 1:200) for 2 h at 37 °C. Nuclei were stained with 4′,6-diamino-2-fenilindol (DAPI; Invitrogen) and preparations were analysed using a confocal microscope (Leica TSC SPE/SP5).

2.5.3. Karyotyping

Karyotype of hESCs was evaluated using G-banded metaphase karyotype analysis. Seventy per cent confluent hESC colonies were treated with colcemid (Thermo Fisher) for 3 h. The cells were then trypsinised, incubated with hypotonic solution (Gibco) and fixed in Carnoy fixative (methanol:acetic acid 3:1). Karyotype was performed following standard procedures (European Guidelines for Constitutional Cytogenetics Analysis 2018).

2.5.4. Alkaline phosphatase assay

The Alkaline Phosphatase (ALP) assay was performed using a two-component buffered ALP substrate containing a BCIP (5-bromo-4-chloro-3-indolyl phosphate) analogue and nitro blue tetrazolium (NBT) (Sigma). hESC colonies were fixed with 4 % PFA for 1 min. Then, they were washed twice with 1× PBS and washed twice again with a 1:1 mixture of both components. Finally, fixed colonies were incubated in the same mixture for a maximum of 10 min. Images of blue-stained pluripotent colonies were obtained using an Olympus IX71 inverted microscope.

2.6. Clonogenicity and doubling time assays

For the clonogenicity assay, 5000 cells were seeded in three wells on iHFFs. Three days after plating for 2iF cultures or 6–7 days for standard medium cultures, the number of colonies per well was assessed and single-cell clonogenicity was expressed as the number of colonies per well over the number of plated cells.

For the doubling time assay, cells were seeded in two wells and collected during the exponential growth phase at 4–5 days of culture (initial time point) and 42–60 h later (final time point). The initial and final numbers of cells were determined using a Neubauer chamber and the doubling time was calculated using the following formula:

$$DT = \frac{time \times log(2)}{log\left(\frac{final\ number\ of\ cells}{initial\ number\ of\ cells}\right)}$$

2.7. TFE3 intracellular localization analysis

Cells were fixed and immunostained using the aforementioned protocol. Antibodies used were a rabbit polyclonal anti-TFE3 primary antibody (Sigma, HPA023881, dilution 1:200) and a goat anti-rabbit IgG Alexa Fluor 594 secondary antibody (Molecular Probes, A-11037, dilution 1:500).

The ImageJ software was used to calculate the nuclear vs cytoplasmatic ratios of TFE3 staining in images obtained using an inverted epifluorescence microscope (Olympus). Nuclei and surrounding cytoplasmic regions were selected and the mean grey value (MGV) was measured for the two compartments of each cell. The TFE3 ratio was measured in 100 cells from several colonies of each hESC line.

2.8. Mitochondrial activity analysis

Mitochondrial membrane potential was quantified using the tetramethylrhodamine ethyl ester (TMRE) mitochondrial membrane potential assay kit (Abcam) following the manufacturer's instructions. Images were obtained using an inverted epifluorescence microscope (Olympus) and the mean fluorescence intensity was quantified as the MGV of a minimum of 10 colonies from each hESC line using the ImageJ software.

2.9. DNA extraction and 5mC/5hmC quantification

Several hESC colonies were mechanically separated from the feeder cells and genomic DNA was extracted using the Gentra Puregene Cell Kit (Qiagen) following the manufacturer's instructions. Its concentration and purity were assessed using a Nanodrop spectrophotometer (Thermo Fisher).

To quantify 5-methylcytosine (5mC) and 5-hydroxymethylcytosine (5hmC), the Fluorometric Methylated DNA Quantification Kit (Abcam) and the Fluorometric Hydroxymethylated DNA Quantification Kit (Abcam) were used, respectively, following the manufacturer's instructions. Relative Fluorescence Units were measured in duplicate using a Spark® multimode microplate reader (Tecan) at 530 nm excitation/590 nm emission.

2.10. Embryoid body formation

bm- and bc-hESC colonies were mechanically disaggregated into medium-sized cell clumps and cultured in Nunclon Sphera 12-well plates (Thermo Fisher) in hESC medium without bFGF. Naïve-converted hESCs colonies were trypsinised and seeded in the same 12-well plates in hESC medium without bFGF, PD, or CH. The medium was changed every other day and embryoid bodies (EBs) were cultured in suspension for six days.

2.11. RNA extraction and real-time quantitative PCR

For the gene expression analysis of core, primed, and naïve pluripotency markers, hESC colonies were mechanically separated from the feeder cells. For the differentiation analysis, 6-day old EBs were isolated.

Total RNA from both hESCs and EBs was isolated using the Maxwell® RSC simplyRNA Tissue Kit (Promega), following the manufacturer's instructions.

RNA concentration and purity were assessed using a Nanodrop

spectrophotometer (Thermo Fisher). Then, 1 µg of total RNA was reverse-transcribed (RT) to cDNA using the iScript cDNA Synthesis Kit (Bio-Rad). The RT reaction was performed as follows: 5 min at 25 °C, 30 min at 42 °C, 5 min at 85 °C, and cooling to 4 °C.

For the expression analysis of core, primed and naïve pluripotency markers, five nanograms of cDNA were used in a total reaction volume of 20 µl per well. Primers were either selected from the literature or designed in-house (Table S1). All primers were tested and those with efficiency values ranging from 90 to 115 % were validated. *GAPDH*, *RPL13A*, and *RPLP0* were used as housekeeping genes for normalization. A non-template control (NTC) was added for each gene.

For the expression analysis of differentiation genes, five nanograms of cDNA were used in a total reaction volume of 10 µl per well. Validated PrimePCR SYBR green assays (Bio-Rad) for pluripotency and lineage markers were used. *GAPDH* and *RPLP0* were used as housekeeping genes for normalization. A NTC was added for each gene.

In both experiments, the reaction program consisted of a denaturation step of 3 min at 95 °C followed by 40 cycles of 5 s at 95 °C (denaturing) and 30 s at 60 °C (annealing and extension). The melt curve of the reaction products was obtained with a final step consisting of an increment of 0.5 °C every 5 s from 65 °C to 95 °C.

2.12. Library preparation and RNA-sequencing

Two micrograms of total RNA obtained from each hESC line was sent to the Centre Nacional d'Anàlisi Genòmica (CNAG) in Barcelona (Spain) for RNA sequencing (RNA-seq).

Total RNA was quantified using a Qubit® RNA BR Assay kit (Thermo Fisher Scientific) and RNA integrity was estimated using an RNA 6000 Nano Bioanalyzer 2100 Assay (Agilent).

RNA-seq libraries were prepared with the KAPA Stranded mRNA-Seq Illumina Platform Kit (Roche) following the manufacturer's recommendations. Briefly, 500 ng of total RNA was used for poly-A fraction enrichment with oligo-dT magnetic beads, following mRNA fragmentation by divalent metal cations at high temperature. Strand specificity was achieved during the second strand synthesis performed in the presence of dUTP instead of dTTP. The blunt-ended double-stranded cDNA was 3′adenylated and Illumina platform-compatible adaptors with unique dual indexes and unique molecular identifiers (Integrated DNA Technologies) were ligated. The ligation product was enriched with 15 PCR cycles and the final library was validated using an Agilent 2100 Bioanalyzer with a DNA 7500 assay.

The libraries were sequenced on a NovaSeq 6000 (Illumina) in paired-end mode with a read length of 2 × 51 bp, following the manufacturer's protocol for dual indexing. Image analysis, base calling, and quality scoring of the run were processed using the manufacturer's software Real Time Analysis (RTA 3.4.4), followed by the generation of FASTQ sequence files.

2.13. RNA-seq processing and analysis

RNA-seq reads were mapped against the human reference genome (GRCh38) using the STAR software version 2.7.8a (Dobin et al., 2013) with ENCODE parameters. Annotated genes were quantified with RSEM v1.3.0 (Li and Dewey, 2011) using default parameters and the human GENCODE annotation version 38.

A Principal Component Analysis (PCA) plot was generated with regularized log-transformed (rlog) counts, taking all genes into account. A heatmap with the top 50 differentially expressed (DE) genes was generated using the pheatmap R package, using the scaled rlog-transformed counts.

Differential expression gene (DEG) analysis was performed with DESeq2 v1.36.0 R package (Love et al., 2014) using a Wald test to compare the bm-hESC and bc-hESC groups. Genes were considered differentially expressed with an adjusted p-value <0.05 and absolute fold change $|FC| > 1.5$. Significant genes were selected for Gene Ontology (GO) enrichment analysis using the PANTHER software. A PANTHER overrepresentation test was performed on the GO Ontology database (DOI: https://doi.org/10.5281/zenodo.6799722) released on July 1st, 2022, applying a Fisher's exact test with False Discovery Rate correction.

2.14. Experimental design

Three experimental groups were defined for hESC derivation from both blastomeres and blastocysts. In the CHY group, embryos were cultured in the presence of CH and Y from the 4-cell stage until plating onto iHFFs. The same inhibitors were then added to the hESC culture medium. Y and CH were removed at day 6 and 12, respectively. bFGF was added either at day 0 or 6. To determine the effect of embryo culture with CH and Y on hESC derivation efficiency, we designed a second group, named NT, equivalent to the CHY one, but without inhibitors in the embryo culture medium. Finally, the negative control NT-NT group contained no inhibitors at any step (Fig. 1).

Analyses of naïve pluripotency indicators and qPCR for naïve and primed pluripotency markers were carried out in all four bm-hESCs lines and six bc-hESCs lines (three from the NT group and three from the CHY group), along with the naïve-converted hESC line. All tests were performed at low culture passages (3–5) for bm-hESCs and bc-hESCs to minimize the effect of culture conditions on their pluripotency state, and at passage 12–15 for naïve-converted hESCs. qPCR analyses were repeated at passage 15 in bc-hESCs and bm-hESCs to assess the influence of culture passages on naïve and primed gene expression.

Clonogenicity and doubling time assays were performed in all four bm-ESC lines and in four bc-hESC lines (2 from the NT group and 2 from the CHY group), as well as in the naïve-converted hESC line. Bm-hESCs and bc-hESCs lines were used at low culture passages (3–5) whereas the naïve converted line was used at passage 12–15.

For RNA-seq and germ layer differentiation analyses, all four bm-hESC lines and four bc-hESC lines were used, along with the naïve-converted hESC line. Tests were performed at intermediate culture passages (6–9) for bm-hESCs and bc-hESCs, whereas the naïve-converted line was analysed at passage 15.

2.15. Statistical analysis

Derivation efficiency values for each group were compared using a Fisher's exact test. The TFE3 ratios for each group were compared using a Kruskal-Wallis test followed by Dunn's post-hoc test.

The clonogenicity and doubling time assay values, mean TMRE fluorescence intensity per colony values, and mean percentages of genomic 5mC and 5hmC in each group were compared by performing a one-way ANOVA test followed by a Tukey HSD post-hoc test.

In qPCR experiments, relative expression levels were calculated using the $\Delta\Delta C_q$ method. A one-way ANOVA test followed by Tukey's HSD post-hoc test was applied to the relative expression values of each gene.

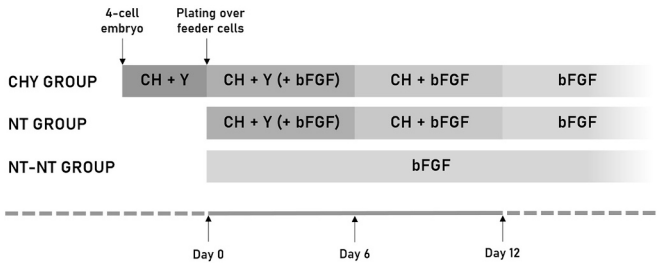

Fig. 1. Representation of the culture conditions for each of the three groups of hESC derivation from blastomeres and blastocysts. CH: CHIR99021, Y: Y-27632, bFGF: basic fibroblast growth factor.

Statistical tests were performed using GraphPad Prism 7 (GraphPad Software Inc.), except for the qPCR results, in which CFX Maestro software (Bio-Rad) was used. Differences with p values lower than 0.05 were considered statistically significant.

3. Results

3.1. Generation of outgrowths and PICMIs from single blastomeres and whole blastocysts

To study the transition between isolated blastomeres plated on feeder cells and the establishment of the ESC line, we assessed the capacity of the blastomeres to form an outgrowth and a PICMI before the cell line was fully established. First, cell division (Fig. 2A) and outgrowth formation (Fig. 2B) rates were assessed. No statistical differences were observed among groups (CHY, NT and NT-NT) in cell division rates, but outgrowth formation rates were significantly higher in the CHY and NT groups than in the NT-NT group (Table 1).

PICMIs were observed in some outgrowths during derivation from single blastomeres. Usually, the PICMI could be first detected as a round-shaped structure with small pluripotent-like cells at day 6–7 and kept growing until the first passaging on day 10–12 (Fig. 2C). The PICMI was mechanically separated from the rest of the outgrowth and plated in another well over fresh iHFFs. After the first passage, pluripotent cells began to emerge from the PICMI (Fig. 2D) and eventually formed a hESC colony. Five PICMIs originated from single blastomeres, most of them (4/5) in the CHY group. In our hands, four out of these five PICMIs (80 %) gave rise to a hESC line. Fifteen PICMIs were formed from whole blastocysts, 11 of which (73.3 %) turned into a hESC line. No hESC lines could be derived from single blastomeres nor whole blastocysts without previous PICMI formation (Table 1).

3.2. Effects of GSK3βi, ROCKi and bFGF on hESC derivation efficiencies from single blastomeres and whole blastocysts

Four hESC lines were generated from isolated blastomeres ($n = 508$): three in the CHY group (1.5 %) and one in the NT group (0.6 %). No hESC lines could be derived in the control group (NT-NT), despite the equivalent number of plated blastomeres in each group (Table 2). All four bm-hESC lines were obtained from blastomeres isolated from 8-cell embryos.

The need for exogenous bFGF for bm-hESC derivation was tested by adding it either from day 0 (simultaneously with blastomere plating) or day 6. The highest bm-hESC derivation efficiency was achieved in the CHY group when adding bFGF from day 0, with 3 hESC lines out of 83 blastomeres (3.6 %). Therefore, bFGF was added from day 0 in all groups of hESC derivation from whole blastocysts. No significant differences were observed among groups in terms of derivation efficiency from whole blastocysts. Five bc-hESC lines were established in the CHY group (22.7 %), 4 in the NT group (15.4 %) and 2 in the NT-NT group (8 %) (Table 2).

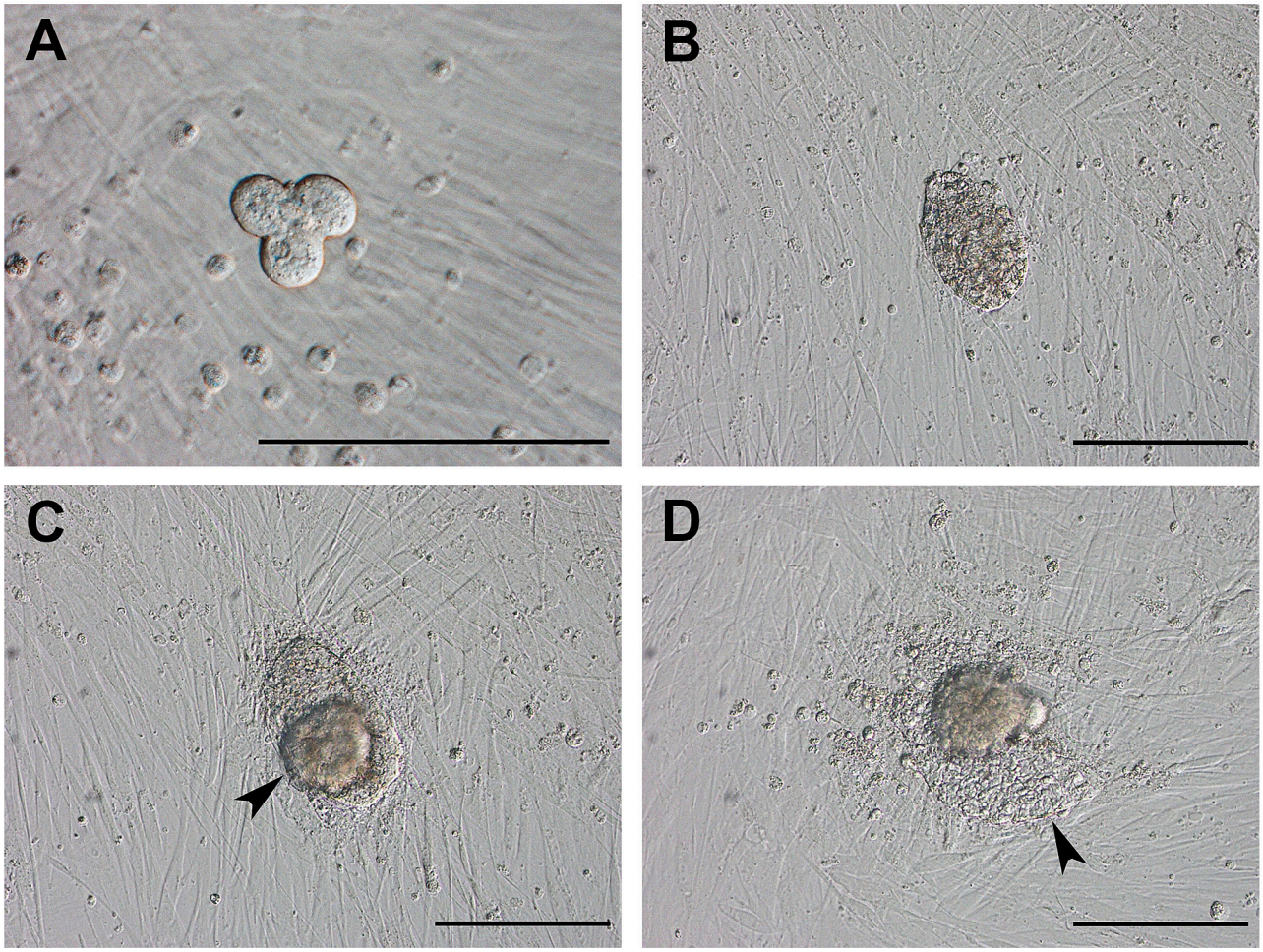

Fig. 2. Initial steps of the hESC derivation process from a single blastomere and PICMI formation, corresponding to the bm-23.3 line from the CHY group. A) Single blastomere seeded onto iHFF, which divided into 3 cells after 48 h in culture. B) Formation of the initial outgrowth at day 5. C) PICMI at day 7. D) hESC-like cells (arrow) growing from the PICMI after mechanical passaging. Scale bars: 200 μm.

Table 1
Outgrowths and PICMI formation and hESC derivation efficiencies from single blastomeres.

		Plated blastomeres	Cell division	Outgrowths	PICMIs	hESC lines
CHY group	bFGF from day 6	115	81 (70.4 %)	32 (27.8 %)	1 (0.9 %)	0
	bFGF from day 0	83	52 (62.7 %)	15 (18.1 %)	3 (3.6 %)	3 (3.6 %)
	Total	198	133 (67.2 %)	47 (23.7 %)[a]	4 (2,0 %)	3 (1.5 %)
NT group	bFGF from day 6	120	85 (70.8 %)	19 (15.8 %)	1 (0.8 %)	1 (0.8 %)
	bFGF from day 0	56	29 (51.8 %)	4 (7.1 %)	0	0
	Total	176	114 (64.8 %)	23 (13.1 %)[b]	1 (0.6 %)	1 (0.6 %)
NT-NT group	bFGF from day 0	134	78 (58.2 %)	2 (1.5 %)[c]	0	0

[a–c]Different letters indicate significant differences between CHY, NT, and NT-NT groups with $p < 0.05$.

Table 2
Outgrowths and PICMI formation and hESC derivation efficiencies from whole blastocysts.

	Plated blastocysts	Outgrowths	PICMIs	hESC lines
CHY group	22	21 (95.5 %)	5 (22.7 %)	5 (22.7 %)
NT group	26	26 (100 %)	4 (15.4 %)	4 (15.4 %)
NT-NT group	25	23 (92 %)	6 (24 %)	2 (8 %)

3.3. Characterization of hESC lines

All putative hESC lines expressed pluripotency markers OCT4, SOX2, and SSEA3 (Fig. 3A–C) and were positive for ALP (Fig. 3G). They were also positive for differentiation markers AFP (endoderm), α-SMA (mesoderm), and TUJ1 (ectoderm) after culture in differentiation-prone conditions (Fig. 3D–F). These results confirmed the pluripotency of these cells.

Most cell lines were chromosomally normal, except for line bm-6.1, which presented an aneuploid karyotype (48,XY,+16,+20) (Fig. 3H, I), and line bc-17, with 85 % mosaicism of trisomy 22 (47,XY,+22/46,XY). Regarding sex, all four bm-hESC lines were male whereas out of the eight bc-hESC lines analysed, three were male and five were female.

3.4. hESC morphology and behaviour in culture

Both bm-hESCs and bc-hESCs formed large, flattened colonies from the second passage onwards (Fig. 4A, B). Most colonies remained undifferentiated with well-defined edges, although a few colonies began to show differentiation at the centre after 5–6 days. By contrast, naïve-converted hESCs in 2iF medium formed small dome-shaped colonies and did not show signs of differentiation after >25 passages (Fig. 4C).

Bm-hESCs showed significantly higher single-cell clonogenicity than bc-hESCs (1.9 % ± 0.6 vs. 0.8 % ± 0.6), although significantly lower than that of naïve-converted hESCs (12.9 %) (Fig. 4D). No differences in cell doubling times were observed between bm-hESCs and bc-hESCs (30.6 h ± 2.9 vs. 32.4 h ± 2.6), whereas naïve-converted hESCs proliferated significantly faster (16.2 h) (Fig. 4E).

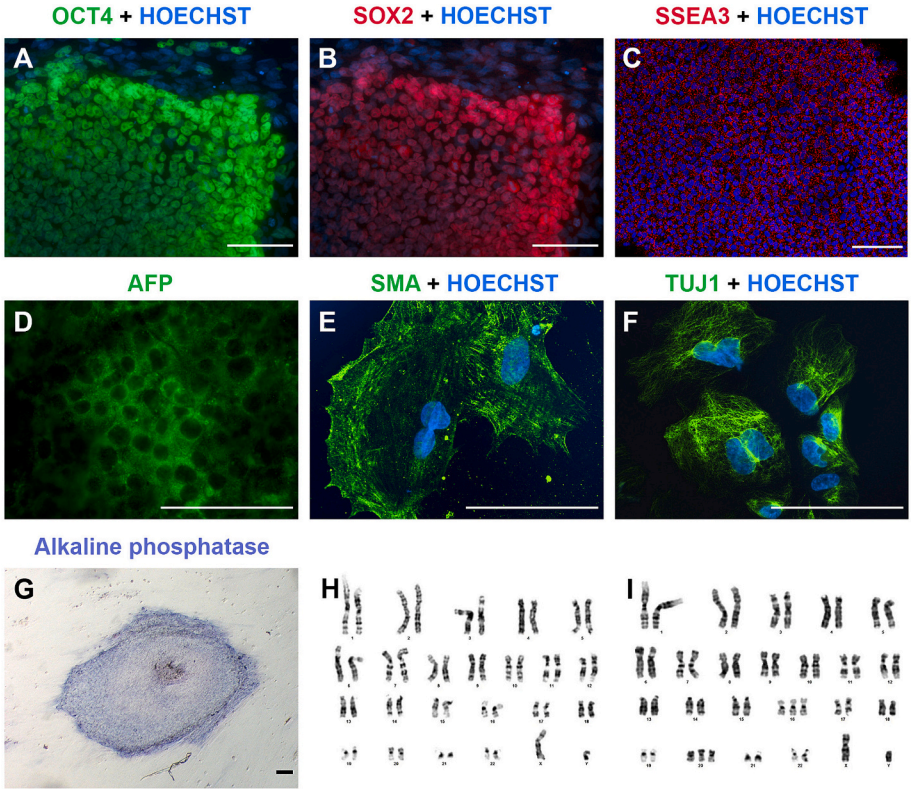

Fig. 3. Characterization of putative hESC lines. A–C) Immunofluorescence detection of pluripotency markers OCT4 (green), SOX2 (red) and SSEA-3 (red). Nuclei were counterstained with Hoechst 33258 (blue). D–F) Immunofluorescence detection of differentiation markers AFP (endoderm; green), SMA (mesoderm; green) and TUJ1 (ectoderm; green). Nuclei were counterstained with Hoechst 33258 (blue). G) Image of a hESC colony after the alkaline phosphatase assay. H) Karyotype of the bm-31.5 line at passage 14. I) Karyotype of the bm-6.1 line at passage 16. Scale bars: 200 μm.

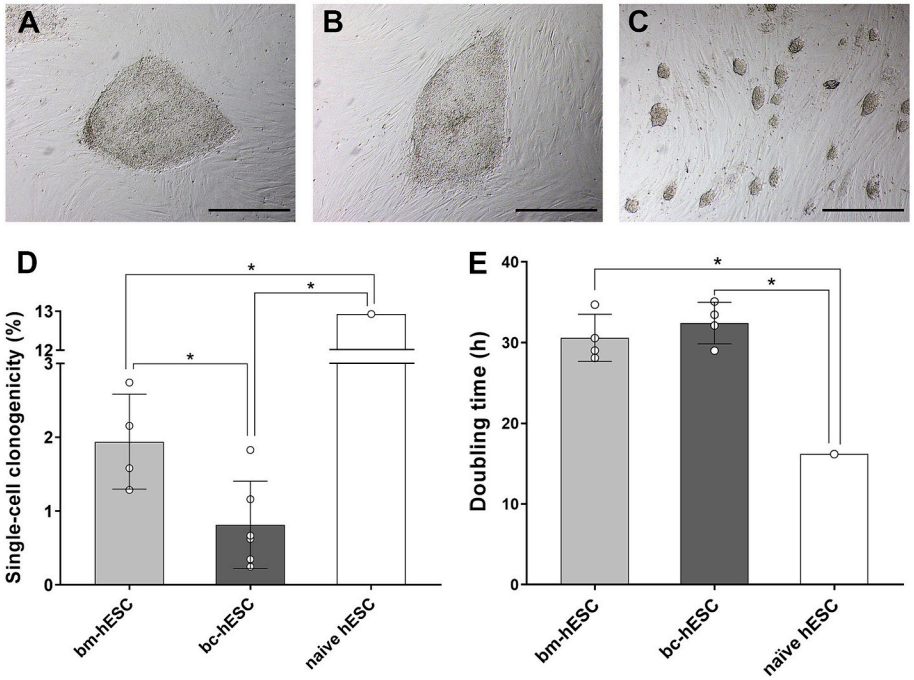

Fig. 4. hESC colony morphology and behaviour in culture. A–C) Images of hESC colonies from a blastomere-derived hESC line (bm-23.3), a blastocyst-derived hESC line (bc-8) and a naïve-converted hESC line (ES[10]), respectively. Scale bar: 500 μm. D) Single-cell clonogenicity expressed as number of colonies out of number of plated cells. Each dot represents a cell line. E) Mean cell population doubling time. Each dot represents a hESC line. Mean ± SD, $*p < 0.05$.

3.5. Analysis of naïve pluripotency indicators

TFE3 showed a preferential cytoplasmic localization in all bm-hESCs and bc-hESCs lines analysed, whereas naïve-converted cells exhibited nuclear enrichment of TFE3 (Fig. 5A). Fluorescence quantification confirmed no significant differences in the nuclear vs cytoplasmic ratios of TFE3 between bm-hESCs and bc-hESCs (0.59 ± 0.16 vs 0.59 ± 0.22, respectively), whereas this ratio was significantly higher in the naïve-converted hESC line (1.80 ± 0.42) (Fig. 5B).

In terms of mitochondrial activity, bm-hESCs and bc-hESCs showed no significant differences in the intensity of TMRE staining (26.5 ± 4.1 vs. 25.7 ± 4.0, respectively), whereas it was significantly more intense in the naïve-converted hESC line (35.0 ± 5.2) (Fig. 5C, D), indicating a higher mitochondrial membrane polarization.

Finally, no significant differences were found in the genomic 5mC levels between bm-hESCs and bc-hESCs (2.9 % ± 0.3 vs. 2.8 % ± 0.3), nor in 5hmC levels (0.038 % ± 0.006 vs. 0.043 % ± 0.008, respectively). Naïve converted hESCs showed significantly lower levels of methylated cytosines (1.7 %) and also lower levels of 5hmC (0.028 %), although this latter difference was not statistically significant (Fig. 5E, F).

3.6. Expression of naïve and primed pluripotency genes

No significant differences were found in the expression of the core pluripotency marker OCT4 among bm-hESC, bc-hESC and the naïve converted hESC at passage 5 nor at passage 15, whereas naïve hESCs showed a higher expression of SOX2 at both passages (Fig. 6A, D). At passage 5, the expression of the naïve marker DNMT3L was significantly higher in bm-hESCs than in bc-hESCs, although lower than in the naïve-converted positive control line. The expression of naïve markers PRDM14, REX1, and STELLA in bm-hESCs was also higher than in bc-hESCs, but equivalent to the naïve-converted positive control (Fig. 6B). Most of these differences disappeared at passage 15, when only the expression of DNMT3L, which remained significantly higher in bm-hESCs and became equivalent to the naïve-converted line (Fig. 6E). None of the hESC lines expressed detectable KLF17 levels (data not shown). As for primed markers, no significant differences were observed among the three groups neither at passage 5 nor at passage 15 (Fig. 6C, F). Additionally, when comparing the expression levels of naïve and primed pluripotency genes in bm-hESCs at passage 15 with those at passage 5, we observed that the expression of REX1 and STELLA significantly decreased at passage 15 (data not shown).

3.7. Transcriptome analysis

PCA showed that all bm-hESC and bc-hESC lines clustered together, except for the bc-4 line, and separated from the naïve-converted hESC line (Fig. 7A). An effect of the sex of the hESC lines was observed in the PC1vsPC3 representation of the PCA, in which all XY lines clustered together and separated from the XX lines (Fig. 7B). The bm-hESCs group included only XY lines, whereas the bc-hESCs group had two XY (bc-17 and bc-21) and two XX (bc-4 and bc-26) hESC lines. The transcript with the highest contribution to the variability explained by PC3 was *XIST*, along with many genes located in the Y chromosome (Table S2). The presence of *XIST* among this set of transcripts was expected since the female lines from the bc-hESC group showed X-chromosome inactivation, as assessed by immunostaining for the H3K27me3 marker (Fig. S1). Therefore, considering the results of the PCA, we opted to include only the genes in autosomes and mitochondria in the DEG analysis. When applying this correction, the distribution of the hESC lines in the PC1vsPC2 (Fig. 7C) was similar to the distribution of the hESC lines considering all genes (Fig. 7A) but hESC lines did not cluster by their sex in the PC1vsPC3 representation (Fig. 7D).

3.8. Differential expression gene analysis

DEG analysis considering only autosomal and mitochondrial genes of the bm-hESC and bc-hESC lines showed a total of 78 DE genes with fold change ≥1.5 and $p < 0.05$. Of these, 57 genes were upregulated in bc-hESCs, and 21 were upregulated in bm-hESCs (Table S3). The heatmap represents the top 50 DE genes between bm-hESCs and bc-hESCs (Fig. 8A). The GO analysis revealed several GO biological process

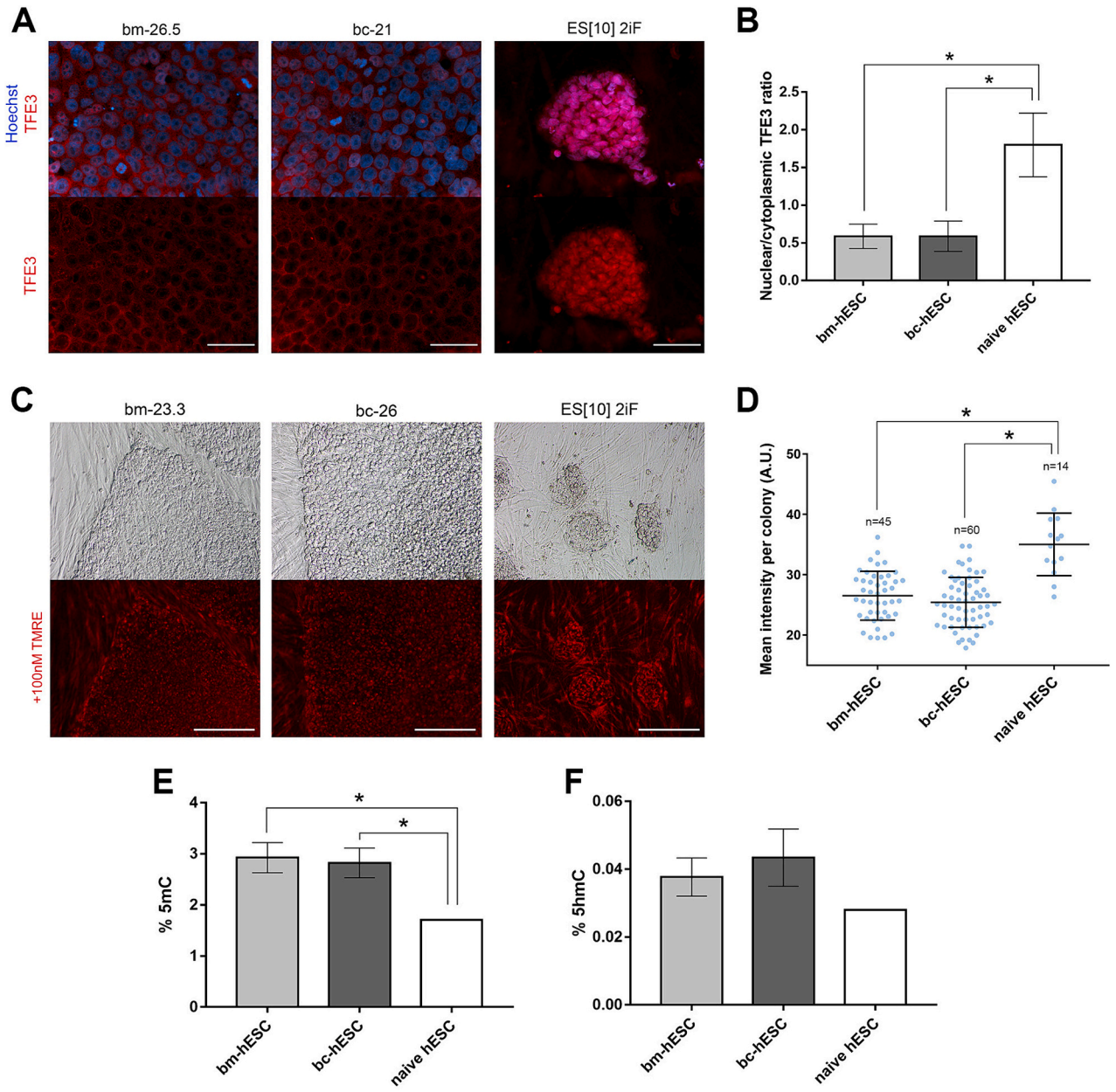

Fig. 5. Analysis of naïve pluripotency indicators. A) Representative images of immunofluorescence detection of TFE3 (red) counterstained with Hoechst 33258 (blue) in a bm-hESC line (bm-26.5), a bc-hESC line (bc-21) and a naïve-converted hESC line (ES[10]2iF). Scale bars: 100 μm. B) Fluorescence quantification of the TFE3 immunofluorescence. Expressed as mean ± SD. C) Representative images of TMRE staining (red) in a bm-hESC line (bm-23.3), a bc-hESC line (bc-26) and a naïve-converted hESC line (ES[10]2iF). Scale bars: 200 μm. D) Fluorescence quantification of the TMRE staining. Each point represents a single hESC colony, and all lines from each group are equally represented. Expressed as mean ± SD. E) Quantification of global 5mC. F) Quantification of global 5hmC. *p < 0.05.

terms significantly overrepresented among the DE genes upregulated in bc-hESCs with p < 0.05. Eighteen genes were related to the GO term "nervous system development" and nine genes were related to "pattern specification process", including six genes involved in "anterior-posterior pattern specification" and four in "somite development" (Fig. 8B). Regarding the 21 transcripts overrepresented in bm-hESCs, 13 constituted protein-coding genes, and the GO analysis did not find any GO biological process significantly enriched.

Finally, we compared the expression levels of an array of core, primed and naïve pluripotency marker genes described by Taei et al. (Taei et al., 2020). Considering only these genes, the bm- and bc-hESC lines clustered according to the developmental stage of their source embryo, with the only exception of the bm-26.5 line (Fig. S2).

3.9. Primary germ layer differentiation capacity of hESCs by EBs formation

To evaluate whether the differences observed at the transcriptome level between bm-hESC and bc-hESC lines can affect their ability to differentiate into cells of the three primary germ layers, we quantified the changes in the expression of several lineage markers after spontaneous differentiation of the bm-hESCs, bc-hESCs, and the naïve-converted hESC line to EBs for 6 days (Fig. 9A). The qPCR results indicated that, when treated as a whole, no significant differences existed between the three groups in the expression levels of pluripotent, ectodermal, mesodermal and endodermal markers of the EBs relative to the undifferentiated hESCs (Fig. 9B). However, large heterogeneity was observed between the different hESC lines, even within the same experimental

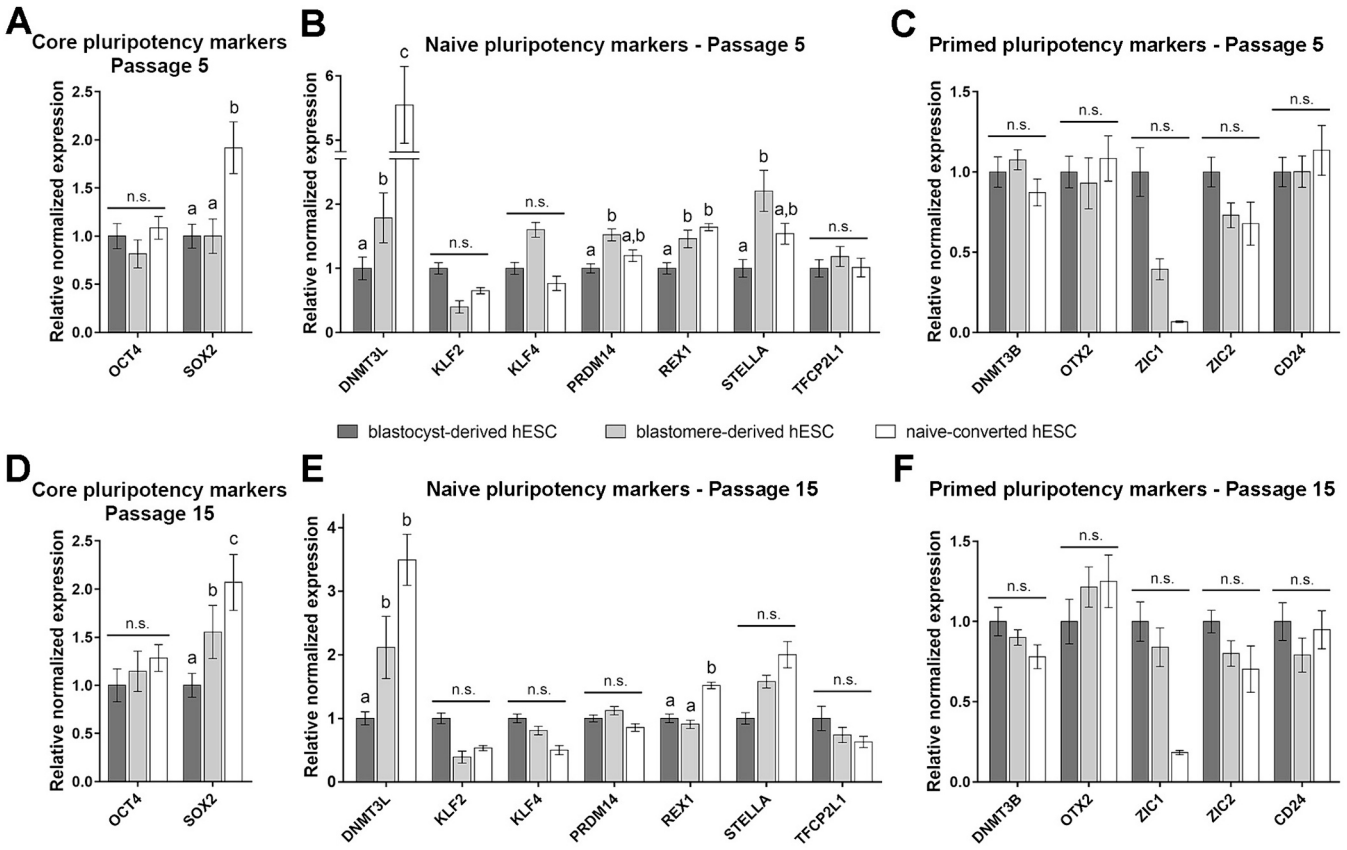

Fig. 6. qPCR results of the expression of core, naïve and primed pluripotency genes in bc-hESCs, bm-hESCs and naïve-converted hESCs. Expressed as mean ± SD A–C) Expression of core, naïve and primed pluripotency genes at passage 5. D–F) Expression of core, naïve and primed pluripotency genes at passage 15. Different letters indicate statistically significant differences among the three groups of lines with $p < 0.05$.

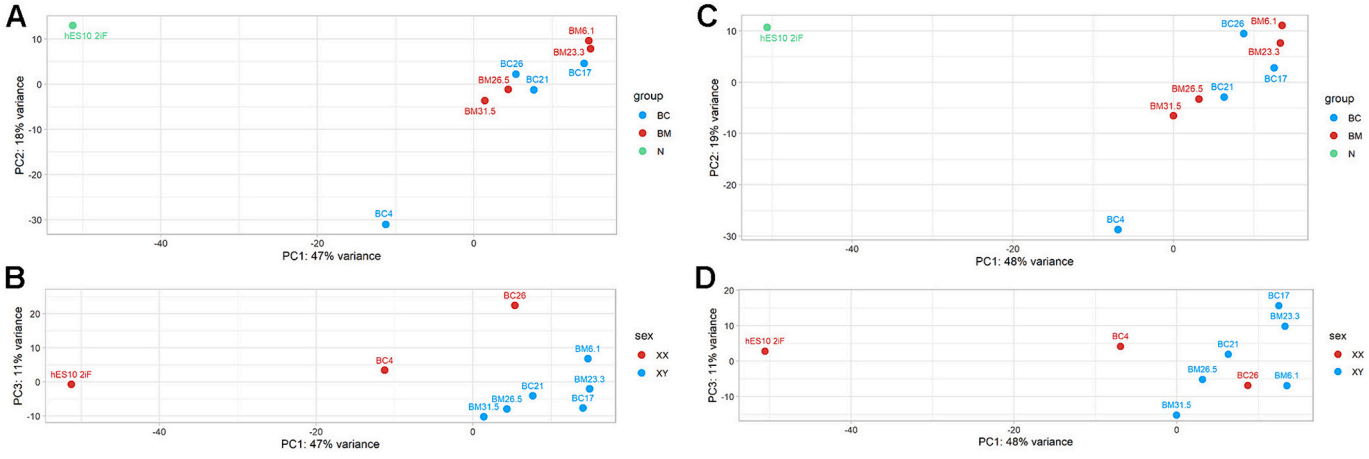

Fig. 7. Principal Component Analysis (PCA) of the bm-hESC lines (bm-6.1, bm-23.3, bm-26.5 and bm-31.5), bc-hESC lines (bc-4, bc-17, bc-21 and bc-26) and the naïve hESC line hES10 2iF. A–B) PC1vsPC2 and PC1vsPC3 representation including all genes. C–D) PC1vsPC2 and PC1vsPC3 representation including only autosomal and mitochondrial genes.

group. This heterogeneity was already observed when comparing the different hESC lines before differentiation (Fig. S3).

Statistically significant differences in the expression of pluripotency and lineage markers were also detected among the EBs generated relative to their corresponding hESCs. Lines bm-6.1, bm-23.3, bc-21, and bc-26 differentiated efficiently towards the three germ layers. Lines bm-26.5 and bc-17 showed efficient differentiation only towards mesoderm and endoderm. Lines bm-31.5 and bc-4 differentiated well only towards mesoderm, although the upregulation of mesoderm markers was milder compared to other hESC lines. Lastly, the naïve-converted hESC line upregulated all lineage markers except *FOXA2* after differentiation, but the increase in gene expression was lower than that observed in other lines (Fig. 9C–E). Regarding pluripotency markers, in the bm-hESC group, line bm-6.1 downregulated both *OCT4* and *SOX2* after differentiation, lines bm-26.5 and bm-31.5 downregulated only *SOX2*, and no downregulation of any of the two markers was detected in line bm-23.3. In the bc-hESC group, the pluripotency marker *OCT4* was downregulated in lines bc-4 and bc-21, whereas all lines, except bc-21,

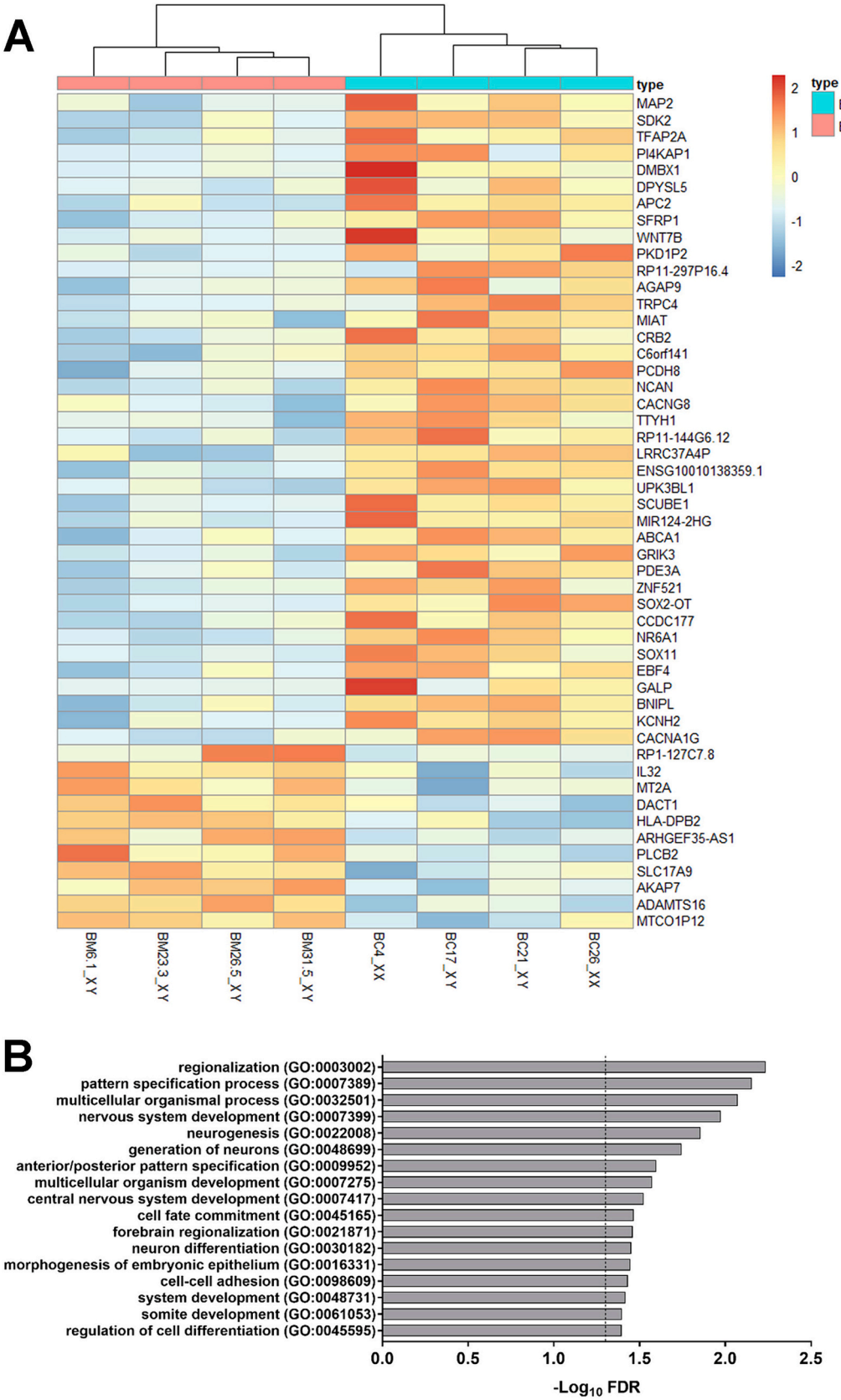

Fig. 8. Differential Expression (DE) and Gene Ontology (GO) analysis. A) Heatmap of the top 50 DE genes between bm-hESCs and bc-hESCs. B) Significantly overrepresented GO biological process terms among the genes upregulated in bc-hESCs. Dashed line marks the significance threshold at $p = 0.05$.

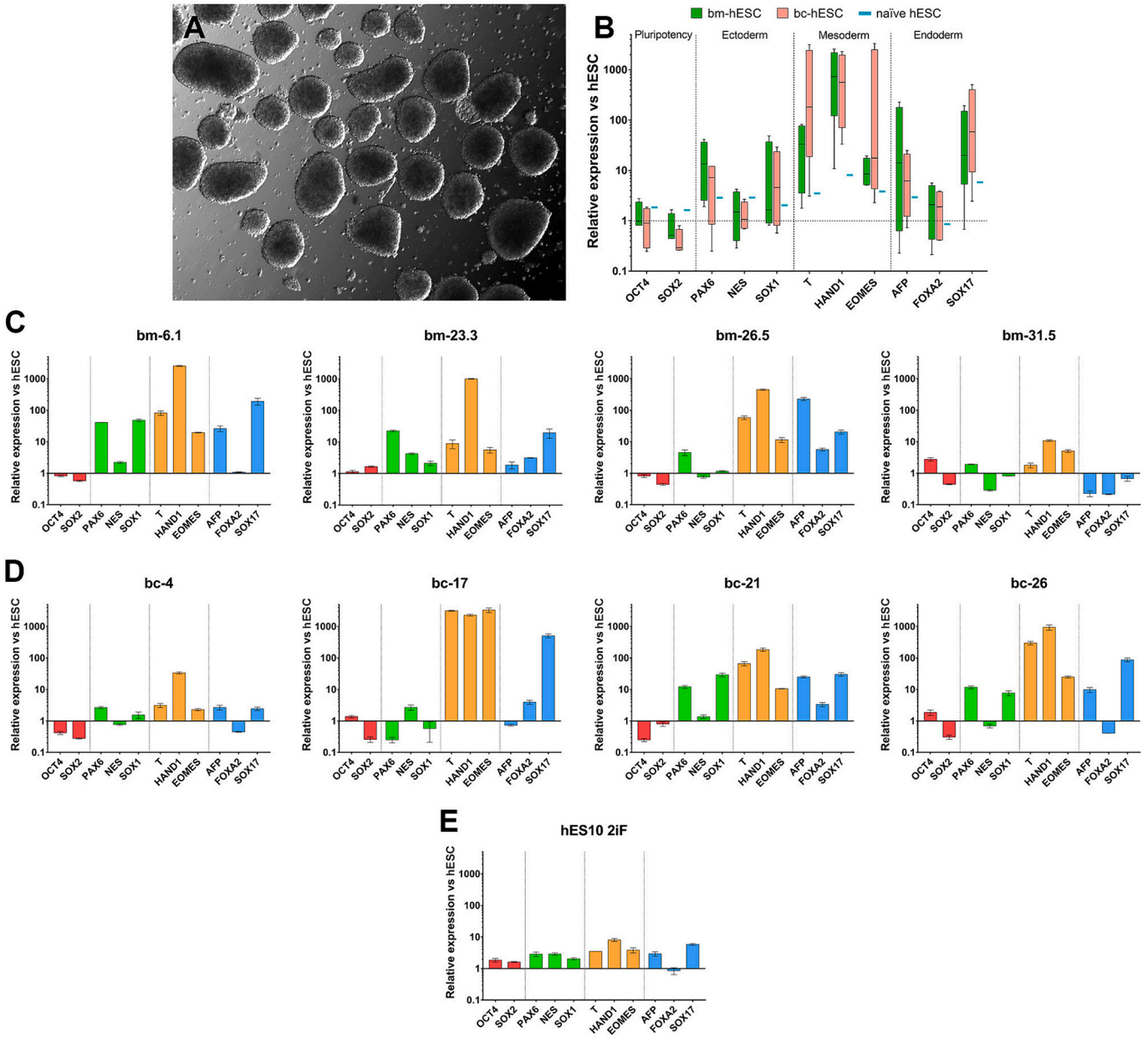

Fig. 9. Differentiation of hESC lines to cells of the three primary germ layers. A) Embryoid bodies (EBs) after 6 days of suspension culture. B) Expression of pluripotency and lineage markers in bm-hESC, bc-hESC and naïve hESC-derived EBs normalized to respective undifferentiated hESCs. C–E) Expression of ectoderm (green), mesoderm (orange) and endoderm (blue) markers in EBs normalized to respective undifferentiated hESCs in bm-hESC lines (C), bc-hESC lines (D) and the naïve-converted hESC line (E).

downregulated *SOX2* after differentiation. The naïve-converted hESC line failed to downregulate any of the pluripotency markers after differentiation (Fig. 9E).

3.10. *hESC derivation from single blastomeres in naïve conditions*

We attempted to derive hESC lines from single blastomeres directly under naïve conditions using the 2iF medium. To maximize efficiency, 4-cell embryos were cultured in the presence of CH + Y until the 8-cell stage, as in the CHY group, and after embryo biopsy single blastomeres were seeded onto feeder cells in 2iF medium. Of the 161 blastomeres plated, 16 formed an outgrowth (10 %) and three of them gave rise to a PICMI (1.9 %). All three PICMIs could be mechanically separated from the non-pluripotent cells of the outgrowth, but they rapidly differentiated after the first passaging and no hESC lines could be obtained.

4. Discussion

In this study, we were able to derive multiple lines of hESCs from both blastocysts and single blastomeres of 8-cell embryos and to characterize their pluripotency state using a comprehensive set of cellular and molecular analyses.

Regarding hESCs derivation, we report, for the first time, the formation of PICMIs from single human blastomeres. Our results support the hypothesis that PICMI formation is essential for the establishment of a new hESC line not only from blastocysts, as previously described (O'Leary et al., 2012), but also from single blastomeres. Thus, although blastomeres formed outgrowths without going through the blastocyst stage, they subsequently underwent morphological changes similar to those of whole blastocysts during hESC derivation under the same culture conditions.

Our results also confirm that the use of GSK3β inhibitor CH and ROCK inhibitor Y has a beneficial effect on the derivation of hESCs from single blastomeres. ROCK inhibitor is known to enhance hESC survival, especially when dissociated as single cells (Watanabe et al., 2007), whereas low concentrations of GSK3β inhibitor maintain hESCs in a pluripotent state and inhibit differentiation (Singh et al., 2012). This is consistent with the results obtained by Taei et al. (Taei et al., 2013), although they reported a higher derivation efficiency (up to 13 %). However, they used mouse embryonic fibroblasts (MEFs) as feeder cells and were not able to establish any hESC line on HFFs. In contrast, our results demonstrate that hESC lines can be derived from single blastomeres by direct plating over HFFs, which are more stable and durable than MEFs (Ma et al., 2012; Meng et al., 2008; Richards et al., 2003) and avoid the presence of xeno-products in the culture medium. Some studies have reported differences between HFFs and MEFs in their production and secretion of growth factors to the culture medium (Eiselleova et al., 2008; Yang et al., 2016), which may explain the lower efficiencies obtained in this study.

Next, we aimed to characterize the pluripotency state of the bm-hESCs lines and compare it with that of known primed bc-hESC lines. Several molecular indicators pointed towards bm-hESCs presenting a state of pluripotency close to the primed state, as similar results in the localization of TFE3, mitochondrial activity, and global DNA methylation and hydroxymethylation levels were observed between bm-hESC and bc-hESC lines. First, TFE3 is known to exit the nucleus at the onset of ESC differentiation (Betschinger et al., 2013), accumulating in the cytoplasm in primed hESCs while being enriched in the nucleus in naïve hESCs (Gafni et al., 2013). Second, it is reported that primed stem cells have a preferentially glycolytic metabolism, showing low mitochondrial activity, whereas naïve stem cells are bivalent, leaning on both glycolysis and oxidative phosphorylation for energy production (Takashima et al., 2014; Sperber et al., 2015; Zhou et al., 2012). Third, it is known that naïve mESCs show a hypomethylated genome with respect to their primed counterparts, and oxidation of 5mC into 5hmC is one of the mechanisms involved in the demethylation observed during the serum to 2i transition (Hackett et al., 2013; Leitch et al., 2013; von Meyenn et al., 2016).

Nonetheless, cell behaviour in culture pointed towards a more naïve pluripotency state of bm-hESCs when compared to bc-hESCs. The fact that bm-hESCs presented a higher single-cell clonogenicity than bc-hESCs implies that a high number of cells could be obtained more rapidly and easily than when using bc-hESCs. Importantly, it should be noted that the bm-6.1 line, which showed the highest clonogenic capacity among all bm- and bc-hESC lines, presented a trisomy 20, and it is known that a gain of the region 20q11.21 confers selective advantage and higher clonogenic capacity to hESCs (Nguyen et al., 2014; Avery et al., 2013). Therefore, we cannot exclude the possibility that the higher clonogenicity observed in this particular hESC line is caused by its abnormal karyotype. Nevertheless, all the other three bm-hESC lines showed a higher clonogenic capacity than 5 of the 6 bc-hESC lines analysed, so an effect of the embryonic origin of the hESC lines is most probably still present.

Similarly, results from qPCR analyses leaned in the same direction, with several markers showing higher expression in bm-hESCs than in bc-hESCs at early passages. *DNMT3L* is strongly upregulated in most naïve hESC populations and contributes to their ability to differentiate into different cell types by maintaining bivalent epigenetic signals that may quickly activate or inhibit different sets of genes (Jenkins and Carrell, 2012). PRDM14 and REX1 are associated with maintenance of naïve pluripotency in mESCs (Kalkan et al., 2017; Grabole et al., 2013; Yamaji et al., 2013) and, although they are expressed in conventional hESCs and are thought to be involved in the core pluripotency circuit (Seki, 2018; Son et al., 2013), most of the human naïve cell populations do upregulate both genes (Taei et al., 2020; Warrier et al., 2017), suggesting that they could also play a role in the maintenance of human naïve pluripotency. Finally, *STELLA* is expressed in the human epiblast but is downregulated during the transition to primed hESCs (Yan et al., 2013). Interestingly, most of the differences in the expression of naïve marker genes between bm-hESCs and bc-hESCs disappeared at passage 15. Altogether, these results indicate that bm-hESCs display a slightly more naïve expression profile than bc-hESCs at low culture passages but become more similar at later passages.

Nevertheless, it is important to note that our control naïve hESCs, generated using the protocol described by Ware et al. (Ware et al., 2014), did not show a marked upregulation of several naïve-associated transcription factors, as previously reported (Theunissen et al., 2014; Taei et al., 2020; Warrier et al., 2017). In fact, they are considered intermediate naïve (Taei et al., 2020). Also notably, our modifications of this protocol, which included the use of KO-DMEM instead of DMEM/F12 and the use of iHFFs instead of MEFs or Matrigel, allowed the generation of naïve hESCs without the need for physiological O_2 conditions.

Regarding RNA-seq experiments, the PCA indicated that, at intermediate culture passages, bm-hESCs and bc-hESCs do not show major differences in their transcriptional profiles, and differ from naïve hESCs at the transcriptional level, in line with the outcome of most naïve pluripotency indicators analysed. Nonetheless, bc-hESCs overexpressed a set of genes mainly involved in nervous system development and in embryonic pattern specification with respect to bm-hESCs. Interestingly, both the cynomolgus monkey and the human postimplantation epiblast cell populations of the embryo were found to overexpress genes related to neuron differentiation/nervous system development (Nakamura et al., 2016; Xiang et al., 2020). Moreover, the anterior-posterior axis formation begins at the onset of gastrulation, along with the formation of the primitive streak (Yamaguchi, 2001). Accordingly, genes related to pattern specification processes were found to be overexpressed in gastrulating cynomolgus monkey embryos (Nakamura et al., 2016). Therefore, our GO analysis results suggest that bc-hESCs recapitulate better the very late postimplantation epiblast of the human embryo than bm-hESCs, and that bm-hESCs may closer resemble an earlier stage of the human embryo than bc-hESCs (in agreement with their embryonic source). Additionally, hESC lines clustered by the embryonic stage of their origin regarding the expression of core, naïve and primed pluripotency markers, suggesting an effect of the developmental stage of the source embryo on the pluripotency state of the hESC lines.

A recent study compared the gene expression profiles of XY and XX isogenic hiPSCs and found that female lines showed a pluripotency state closer to the naïve state than male lines (Waldhorn et al., 2022). Therefore, the fact that all our bm-hESC lines were male might also explain the mildness of the differences found between bm-hESCs and bc-hESCs in this study.

Despite these transcriptional differences, bm-hESCs and bc-hESCs displayed a similar differentiation potential towards the three primary germ layers. Naïve hESCs showed a milder upregulation of the differentiation markers than bm-hESC and bc-hESC lines after 6 days, which is consistent with reports indicating that naïve hESCs may need a capacitation or re-priming step for efficient differentiation (Lee et al., 2017; Rostovskaya et al., 2019). Even though bc-hESCs upregulated genes related to nervous system development, an increased differentiation propensity towards ectoderm was not observed. However, we cannot exclude the fact that bc-hESCs could be more poised for terminal differentiation into neuronal precursors, hindering or not their capacity to generate other mature cell types. Additionally, the differences observed among hESC lines in the expression of lineage markers and differentiation potential were not correlated with a distinct developmental stage of their source embryo. In fact, heterogeneity of hESC lines regarding their differentiation capacities has been previously reported, and therefore should be considered an intrinsic characteristic of hESCs (Osafune et al., 2008; Bock et al., 2011; Sun et al., 2018).

Finally, results from the hESC derivation attempts in naïve conditions showed that 2iF medium supported the growth of pluripotent cells from single blastomeres until the formation of the PICMI with a similar

efficiency to that obtained under standard conditions when using GSK3βi and ROCKi. However, these cells were unable to progress further as undifferentiated cells. This suggests that the pluripotent cells of the PICMI may need different culture conditions to self-renew and to form a hESC colony. It also reinforces the hypothesis of the PICMI being the turning point between the naïve pluripotency of the preimplantation embryo and the primed pluripotency of the established hESCs in vitro (van der Jeught et al., 2015; Warrier et al., 2018). The fact that both bm-hESCs and bc-hESCs go through the PICMI stage during the derivation process could explain the mildness of the differences observed between them.

It was proposed that the pluripotency state of ESCs should be seen as a wide continuous spectrum instead of the conventional two-state model of naïve vs primed pluripotency (Smith, 2017). This hypothesis was supported by studies that described intermediate pluripotent states in mouse and human (Kinoshita et al., 2021; Neagu et al., 2020; Yu et al., 2021b). In this context, our results suggest that bm-hESCs would fall into the primed end of the spectrum, but allocated slightly closer to the naïve end of the pluripotency continuum than bc-hESCs. On the other hand, the fact that differences in the expression levels of naïve markers were almost exclusively observed at early passages suggests that they are probably caused by the distinct embryonic origin of bm-hESC (8-cell stage, early preimplantation embryo development) and bc-hESC lines (blastocysts, late preimplantation embryo development) rather than being induced by culture conditions. This situation might reflect an intrinsic higher plasticity in differentiation capacity of cells from early stages of embryo development when compared to later stages, in which some differentiation decisions have already been taken.

5. Conclusion

Our results from the analysis of several naïve pluripotency indicators, RNA-sequencing and trilineage differentiation potential showed that bm-hESCs display a primed pluripotency state, similar to that of bc-hESCs. However, their increased single-cell clonogenicity, their higher expression of some naïve pluripotency markers at early passages and minor differences in their transcriptional profile compared to bc-hESCs suggest that bm-hESCs would be allocated closer to the naïve end of the pluripotency continuum.

Funding

This work was supported by the Department of Research and Universities of the Generalitat de Catalunya (2021 SGR 00122) and the Spanish Ministry of Science and Innovation (PID2020-112557GB-I00 to A.R.-H.). O.M. was beneficiary of a FI-2017 fellowship by Generalitat de Catalunya. L.A.-G. was supported by a FPI predoctoral fellowship from the Spanish Ministry of Economy and Competitiveness (PRE-2018-083257).

CRediT authorship contribution statement

Ot Massafret: Writing – original draft, Visualization, Methodology, Investigation, Formal analysis. **Montserrat Barragán:** Resources, Methodology, Formal analysis. **Lucía Álvarez-González:** Formal analysis. **Begoña Aran:** Investigation. **Beatriz Martín-Mur:** Formal analysis. **Anna Esteve-Codina:** Formal analysis. **Aurora Ruiz-Herrera:** Formal analysis. **Elena Ibáñez:** Writing – review & editing, Validation, Supervision, Resources, Project administration, Methodology, Conceptualization. **Josep Santaló:** Writing – review & editing, Validation, Supervision, Resources, Project administration, Methodology, Conceptualization.

Declaration of competing interest

No competing interests declared.

Data availability

The RNAseq data have been deposited in NCBI's Gene Expression Omnibus under GEO Series accession number GSE233878. Additional information required is available upon request.

Acknowledgements

We thank Hospital Universitari Dexeus, Hospital Quirónsalud, Clínica Sagrada Família and Clínica Eugin for the kind donation of surplus embryos. We also thank Sandra Alonso-Alonso, Jonatan Lucas, and María Jesús Alvarez for their supportive work.

Appendix A. Supplementary data

Supplementary data to this article can be found online at https://doi.org/10.1016/j.cdev.2024.203935.

References

Avery, S., Hirst, A.J., Baker, D., Lim, C.Y., Alagaratnam, S., Skotheim, R.I., Knowles, B.B., 2013. BCL-XL mediates the strong selective advantage of a 20q11.21 amplification commonly found in human embryonic stem cell cultures. Stem Cell Rep. 1 (5), 379–386. https://doi.org/10.1016/J.STEMCR.2013.10.005.

Betschinger, J., Nichols, J., Dietmann, S., Corrin, P.D., Paddison, P.J., Smith, A., 2013. Exit from pluripotency is gated by intracellular redistribution of the bHLH transcription factor Tfe3. Cell 153 (2), 335–347. https://doi.org/10.1016/j.cell.2013.03.012.

Bock, C., Kiskinis, E., Verstappen, G., Gu, H., Boulting, G., Smith, Z.D., Meissner, A., 2011. Reference maps of human ES and iPS cell variation enable high-throughput characterization of pluripotent cell lines. Cell 144 (3), 439–452. https://doi.org/10.1016/J.CELL.2010.12.032.

Chan, Y.S., Göke, J., Ng, J.H., Lu, X., Gonzales, K.A.U., Tan, C.P., Ng, H.H., 2013. Induction of a human pluripotent state with distinct regulatory circuitry that resembles preimplantation epiblast. Cell Stem Cell 13 (6), 663–675. https://doi.org/10.1016/J.STEM.2013.11.015.

Chen, H., Aksoy, I., Gonnot, F., Osteil, P., Aubry, M., Hamela, C., Savatier, P., 2015. Reinforcement of STAT3 activity reprogrammes human embryonic stem cells to naive-like pluripotency. Nat. Commun. 6 (1), 1–17. https://doi.org/10.1038/ncomms8095.

Chung, Y., Klimanskaya, I., Becker, S., Li, T., Maserati, M., Lu, S.J., Lanza, R., 2008. Human embryonic stem cell lines generated without embryo destruction. Cell Stem Cell 2 (2), 113–117. https://doi.org/10.1016/j.stem.2007.12.013.

Dobin, A., Davis, C.A., Schlesinger, F., Drenkow, J., Zaleski, C., Jha, S., Gingeras, T.R., 2013. STAR: ultrafast universal RNA-seq aligner. Bioinformatics 29 (1), 15–21. https://doi.org/10.1093/BIOINFORMATICS/BTS635.

Duggal, G., Warrier, S., Ghimire, S., Broekaert, D., van der Jeught, M., Lierman, S., Heindryckx, B., 2015. Alternative routes to induce Naïve pluripotency in human embryonic stem cells. Stem Cells 33 (9), 2686–2698. https://doi.org/10.1002/STEM.2071.

Eiselleova, L., Peterkova, I., Neradil, J., Slaninova, I., Hampl, A., Dvorak, P., 2008. Comparative study of mouse and human feeder cells for human embryonic stem cells. Int. J. Dev. Biol. 52 (4), 353–363. https://doi.org/10.1387/IJDB.082590LE.

Gafni, O., Weinberger, L., Mansour, A.A., Manor, Y.S., Chomsky, E., Ben-Yosef, D., Hanna, J.H., 2013. Derivation of novel human ground state naive pluripotent stem cells. Nature 504 (7479), 282–286. https://doi.org/10.1038/nature12745.

Galan, A., Diaz-Gimeno, P., Poo, M.E., Valbuena, D., Sanchez, E., Ruiz, V., Simon, C., 2013. Defining the genomic signature of totipotency and pluripotency during early human development. PLoS One 8 (4), e62135. https://doi.org/10.1371/JOURNAL.PONE.0062135.

Geens, M., Mateizel, I., Sermon, K., de Rycke, M., Spits, C., Cauffman, G., van de Velde, H., 2009. Human embryonic stem cell lines derived from single blastomeres of two 4-cell stage embryos. Hum. Reprod. 24 (11), 2709–2717. https://doi.org/10.1093/humrep/dep262.

Geens, M., Seriola, A., Barbé, L., Santalo, J., Veiga, A., Dée, K., Spits, C., 2016. Female human pluripotent stem cells rapidly lose X chromosome inactivation marks and progress to a skewed methylation pattern during culture. Mol. Hum. Reprod. 22 (4), 285–298. https://doi.org/10.1093/MOLEHR/GAW004.

Giritharan, G., Ilic, D., Gormley, M., Krtolica, A., 2011. Human embryonic stem cells derived from embryos at different stages of development share similar transcription profiles. PLoS One 6 (10), e26750. https://doi.org/10.1371/JOURNAL.PONE.0026570.

Grabole, N., Tischler, J., Hackett, J.A., Kim, S., Tang, F., Leitch, H.G., Surani, M.A., 2013. Prdm14 promotes germline fate and naive pluripotency by repressing FGF signalling and DNA methylation. EMBO Rep. 14 (7), 629–637. https://doi.org/10.1038/EMBOR.2013.67.

Guo, G., von Meyenn, F., Santos, F., Chen, Y., Reik, W., Bertone, P., Nichols, J., 2016. Naive pluripotent stem cells derived directly from isolated cells of the human inner cell mass. Stem Cell Reports 6 (4), 437–446. https://doi.org/10.1016/J.STEMCR.2016.02.005.

Guo, G., von Meyenn, F., Rostovskaya, M., Clarke, J., Dietmann, S., Baker, D., Smith, A., 2017. Epigenetic resetting of human pluripotency. Development 144 (15), 2748–2763. https://doi.org/10.1242/DEV.146811.

Hackett, J.A., Dietmann, S., Murakami, K., Down, T.A., Leitch, H.G., Surani, M.A., 2013. Synergistic mechanisms of DNA demethylation during transition to ground-state pluripotency. Stem Cell Reports 1 (6), 518. https://doi.org/10.1016/J.STEMCR.2013.11.010.

Hanna, J., Cheng, A.W., Saha, K., Kim, J., Lengner, C.J., Soldner, F., Jaenisch, R., 2010. Human embryonic stem cells with biological and epigenetic characteristics similar to those of mouse ESCs. Proc. Natl. Acad. Sci. 107 (20), 9222–9227. https://doi.org/10.1073/PNAS.1004584107.

Hu, Z., Li, H., Jiang, H., Ren, Y., Yu, X., Qiu, J., Feng, J., 2020. Transient inhibition of mTOR in human pluripotent stem cells enables robust formation of mouse-human chimeric embryos. Science. Advances 6 (20), eaaz0298. https://doi.org/10.1126/SCIADV.AAZ0298.

Ilic, D., Giritharan, G., Zdravkovic, T., Caceres, E., Genbacev, O., Fisher, S.J., Krtolica, A., 2009. Derivation of human embryonic stem cell lines from biopsied blastomeres on human feeders with minimal exposure to xenomaterials. Stem Cells Dev. 18 (9), 1343–1349. https://doi.org/10.1089/scd.2008.0416.

Jenkins, T.G., Carrell, D.T., 2012. The sperm epigenome and potential implications for the developing embryo. Reproduction 143 (6), 727–734. https://doi.org/10.1530/REP-11-0450.

van der Jeught, M., O'Leary, T., Duggal, G., de Sutter, P., de Sousa Lopes, S.C., Heindryckx, B., 2015. The post-inner cellmass intermediate: implications for stem cell biology and assisted reproductive technology. Hum. Reprod. Update 21 (5), 616–626. https://doi.org/10.1093/humupd/dmv028.

Kalkan, T., Olova, N., Roode, M., Mulas, C., Lee, H.J., Nett, I., Smith, A., 2017. Tracking the embryonic stem cell transition from ground state pluripotency. Development 144 (7), 1221–1234. https://doi.org/10.1242/DEV.142711.

Kinoshita, M., Barber, M., Mansfield, W., Dietmann, S., Nichols, J., Cui, Y., Smith, A., 2021. Capture of mouse and human stem cells with features of formative pluripotency. Stem Cells 28, 453–471.e8. https://doi.org/10.1016/j.stem.2020.11.005.

Klimanskaya, I., Chung, Y., Becker, S., Lu, S.J., Lanza, R., 2006. Human embryonic stem cell lines derived from single blastomeres. Nature 444 (7118), 481–485. https://doi.org/10.1038/nature05142.

Lee, J.-H., Laronde, S., Collins, T.J., Lee, J.B., Mitchell, R.R., Bhatia, M., Benoit, Y.D., 2017. Lineage-specific differentiation is influenced by state of human pluripotency accession numbers GSE95505 Lee et al article lineage-specific differentiation is influenced by state of human pluripotency. Cell Rep. 19, 20–35. https://doi.org/10.1016/j.celrep.2017.03.036.

Leitch, H.G., Mcewen, K.R., Turp, A., Encheva, V., Carroll, T., Grabole, N., Hajkova, P., 2013. Naive pluripotency is associated with global DNA hypomethylation. Nat. Struct. Mol. Biol. 20 (3), 311–316. https://doi.org/10.1038/NSMB.2510.

Li, B., Dewey, C.N., 2011. RSEM: accurate transcript quantification from RNA-Seq data with or without a reference genome. BMC Bioinformatics 12 (1), 1–16. https://doi.org/10.1186/1471-2105-12-323/TABLES/6.

Love, M.I., Huber, W., Anders, S., 2014. Moderated estimation of fold change and dispersion for RNA-seq data with DESeq2. Genome Biol. 15 (12), 1–21. https://doi.org/10.1186/S13059-014-0550-8/FIGURES/9.

Ma, Y., Gu, J., Li, C., Wei, X., Tang, F., Shi, G., Jin, Y., 2012. Human foreskin fibroblast produces interleukin-6 to support derivation and self-renewal of mouse embryonic stem cells. Stem Cell Res Ther 3 (4), 29. https://doi.org/10.1186/SCRT120.

Martí, M., Mulero, L., Pardo, C., Morera, C., Carrió, M., Laricchia-Robbio, L., Belmonte, J. C.I., 2013. Characterization of pluripotent stem cells. Nat. Protoc. 8 (2), 223–253. https://doi.org/10.1038/nprot.2012.154.

Meng, G., Liu, S., Krawetz, R., Chan, M., Chernos, J., Rancourt, D.E., 2008. A novel method for generating xeno-free human feeder cells for human embryonic stem cell culture. Stem Cells Dev. 17 (3), 413–422. https://doi.org/10.1089/SCD.2007.0236.

von Meyenn, F., Iurlaro, M., Habibi, E., Liu, N.Q., Salehzadeh-Yazdi, A., Santos, F., Stunnenberg, H.G., 2016. Impairment of DNA methylation maintenance is the main cause of global demethylation in naive embryonic stem cells. Mol. Cell 62 (6), 848–861. https://doi.org/10.1016/J.MOLCEL.2016.04.025.

Nakamura, T., Okamoto, I., Sasaki, K., Yabuta, Y., Iwatani, C., Tsuchiya, H., Saitou, M., 2016. A developmental coordinate of pluripotency among mice, monkeys and humans. Nature 537 (7618), 57–62. https://doi.org/10.1038/nature19096.

Neagu, A., van Genderen, E., Escudero, I., Verwegen, L., Kurek, D., Lehmann, J., ten Berge, D., 2020. In vitro capture and characterization of embryonic rosette-stage pluripotency between naive and primed states. Nat. Cell Biol. 22 (5), 534–545. https://doi.org/10.1038/s41556-020-0508-x.

Nguyen, H.T., Geens, M., Mertzanidou, A., Jacobs, K., Heirman, C., Breckpot, K., Spits, C., 2014. Gain of 20q11.21 in human embryonic stem cells improves cell survival by increased expression of Bcl-xL. Mol. Hum. Reprod. 20 (2), 168–177. https://doi.org/10.1093/molehr/gat077.

Nichols, J., Smith, A., 2009. Naive and primed pluripotent states. In: Cell Stem Cell. https://doi.org/10.1016/j.stem.2009.05.015 (June 5).

Oldak, B., Wildschutz, E., Bondarenko, V., Comar, M.Y., Zhao, C., Aguilera-Castrejon, A., Hanna, J.H., 2023. Complete human day 14 post-implantation embryo models from naive ES cells. Nature 622 (7983), 562–573. https://doi.org/10.1038/s41586-023-06604-5.

O'Leary, T., Heindryckx, B., Lierman, S., Van Bruggen, D., Goeman, J.J., Vandewoestyne, M., De Sutter, P., 2012. Tracking the progression of the human inner cell mass during embryonic stem cell derivation. Nat. Biotechnol. 30 (3), 278–282. https://doi.org/10.1038/nbt.2135.

Osafune, K., Caron, L., Borowiak, M., Martinez, R.J., Fitz-Gerald, C.S., Sato, Y., Melton, D.A., 2008. Marked differences in differentiation propensity among human embryonic stem cell lines. Nat. Biotechnol. 26 (3), 313–315. https://doi.org/10.1038/nbt1383.

Qin, H., Hejna, M., Liu, Y., Percharde, M., Wossidlo, M., Blouin, L., Ramalho-Santos, M., 2016. YAP induces human naive pluripotency. Cell Rep. 14 (10), 2301–2312. https://doi.org/10.1016/J.CELREP.2016.02.036.

Richards, M., Tan, S., Fong, C., Biswas, A., Chan, W., Bongso, A., 2003. Comparative evaluation of various human feeders for prolonged undifferentiated growth of human embryonic stem cells. Stem Cells 21 (5), 546–556. https://doi.org/10.1634/STEMCELLS.21-5-546.

Rostovskaya, M., Stirparo, G.G., Smith, A., 2019. Capacitation of human naïve pluripotent stem cells for multi-lineage differentiation. Development 146 (7), dev172916. https://doi.org/10.1242/DEV.172916.

Seki, Y., 2018. PRDM14 is a unique epigenetic regulator stabilizing transcriptional networks for pluripotency. Frontiers in Cell and Developmental Biology 6 (12). https://doi.org/10.3389/FCELL.2018.00012.

Singh, A.M., Reynolds, D., Cliff, T., Ohtsuka, S., Mattheyses, A.L., Sun, Y., Dalton, S., 2012. Signaling network cross-talk in human pluripotent cells: a Smad2/3-regulated switch that controls the balance between self-renewal and differentiation. Cell Stem Cell 10 (3), 312–326. https://doi.org/10.1016/J.STEM.2012.01.014.

Smith, A., 2017. Formative pluripotency: the executive phase in a developmental continuum. Development 144 (3), 365–373. https://doi.org/10.1242/DEV.142679.

Son, M.Y., Choi, H., Han, Y.M., Cho, Y.S., 2013. Unveiling the critical role of REX1 in the regulation of human stem cell pluripotency. Stem Cells 31 (11), 2374–2387. https://doi.org/10.1002/STEM.1509.

Sperber, H., Mathieu, J., Wang, Y., Ferreccio, A., Hesson, J., Xu, Z., Ruohola-Baker, H., 2015. The metabolome regulates the epigenetic landscape during naive-to-primed human embryonic stem cell transition. Nat. Cell Biol. 17 (12), 1523–1535. https://doi.org/10.1038/ncb3264.

Sun, C., Zhang, J., Zheng, D., Wang, J., Yang, H., Zhang, X., 2018. Transcriptome variations among human embryonic stem cell lines are associated with their differentiation propensity. PLoS One 13 (2), e0192625. https://doi.org/10.1371/JOURNAL.PONE.0192625.

Taei, A., Hassani, S.N., Eftekhari-Yazdi, P., Rezazadeh Valojerdi, M., Nokhbatolfoghahai, M., Masoudi, N.S., Baharvand, H., 2013. Enhanced generation of human embryonic stem cells from single blastomeres of fair and poor-quality cleavage embryos via inhibition of glycogen synthase kinase β and Rho-associated kinase signaling. Hum. Reprod. 28 (10), 2661–2671. https://doi.org/10.1093/humrep/det309.

Taei, A., Rasooli, P., Braun, T., Hassani, S.N., Baharvand, H., 2020. Signal regulators of human naïve pluripotency. Exp. Cell Res. 389 (2), 111924 https://doi.org/10.1016/J.YEXCR.2020.111924.

Takashima, Y., Guo, G., Loos, R., Nichols, J., Ficz, G., Krueger, F., Smith, A., 2014. Resetting transcription factor control circuitry toward ground-state pluripotency in human. Cell 158 (6), 1254–1269. https://doi.org/10.1016/j.cell.2014.08.029.

Theunissen, T.W., Powell, B.E., Wang, H., Mitalipova, M., Faddah, D.A., Reddy, J., Jaenisch, R., 2014. Systematic identification of culture conditions for induction and maintenance of naive human pluripotency. Cell Stem Cell 15 (4), 471. https://doi.org/10.1016/J.STEM.2014.07.002.

Thomson, J.A., 1998. Embryonic stem cell lines derived from human blastocysts. Science 282 (5391), 1145–1147. https://doi.org/10.1126/science.282.5391.1145.

Valamehr, B., Robinson, M., Abujarour, R., Rezner, B., Vranceanu, F., Le, T., Flynn, P., 2014. Platform for induction and maintenance of transgene-free hiPSCs resembling ground state pluripotent stem cells. Stem Cell Reports 2 (3), 366–381. https://doi.org/10.1016/J.STEMCR.2014.01.014.

Waldhorn, I., Turetsky, T., Steiner, D., Gil, Y., Benyamini, H., Gropp, M., Reubinoff, B.E., 2022. Modeling sex differences in humans using isogenic induced pluripotent stem cells. Stem Cell Reports 17 (12), 2732–2744. https://doi.org/10.1016/j.stemcr.2022.10.017.

Ware, C.B., Nelson, A.M., Mecham, B., Hesson, J., Zhou, W., Jonlin, E.C., Ruohola-Baker, H., 2014. Derivation of naïve human embryonic stem cells. Proc. Natl. Acad. Sci. USA 111 (12), 4484–4489. https://doi.org/10.1073/pnas.1319738111.

Warrier, S., van der Jeught, M., Duggal, G., Tilleman, L., Sutherland, E., Taelman, J., Heindryckx, B., 2017. Direct comparison of distinct naive pluripotent states in human embryonic stem cells. Nat. Commun. 8 (1), 1–10. https://doi.org/10.1038/ncomms15055.

Warrier, S., Taelman, J., Tilleman, L., van der Jeught, M., Duggal, G., Lierman, S., Heindryckx, B., 2018. Transcriptional landscape changes during human embryonic stem cell derivation. Mol. Hum. Reprod. 24 (11), 543–555. https://doi.org/10.1093/molehr/gay039.

Watanabe, K., Ueno, M., Kamiya, D., Nishiyama, A., Matsumura, M., Wataya, T., Sasai, Y., 2007. A ROCK inhibitor permits survival of dissociated human embryonic stem cells. Nat. Biotechnol. 25 (6), 681–686. https://doi.org/10.1038/NBT1310.

Weatherbee, B.A.T., Gantner, C.W., Iwamoto-Stohl, L.K., Daza, R.M., Hamazaki, N., Shendure, J., Zernicka-Goetz, M., 2023. Pluripotent stem cell-derived model of the post-implantation human embryo. Nature 622 (7983), 584–593. https://doi.org/10.1038/s41586-023-06368-y.

Xiang, L., Yin, Y., Zheng, Y., Ma, Y., Li, Y., Zhao, Z., Li, T., 2020. A developmental landscape of 3D-cultured human pre-gastrulation embryos. Nature 577 (7791), 537–542. https://doi.org/10.1038/S41586-019-1875-Y.

Yamaguchi, T. P. (2001). Heads or tails: Wnts and anterior-posterior patterning. Curr. Biol., 11, 713–724. Retrieved from http://www.stan-.

Yamaji, M., Ueda, J., Hayashi, K., Ohta, H., Yabuta, Y., Kurimoto, K., Saitou, M., 2013. PRDM14 ensures naive pluripotency through dual regulation of signaling and epigenetic pathways in mouse embryonic stem cells. Cell Stem Cell 12 (3), 368–382. https://doi.org/10.1016/J.STEM.2012.12.012.

Yan, L., Yang, M., Guo, H., Yang, L., Wu, J., Li, R., Tang, F., 2013. Single-cell RNA-Seq profiling of human preimplantation embryos and embryonic stem cells. Nat. Struct. Mol. Biol. 20 (9), 1131–1139. https://doi.org/10.1038/nsmb.2660.

Yang, G., Mai, Q., Li, T., Zhou, C., 2013. Derivation of human embryonic stem cell lines from single blastomeres of low-quality embryos by direct plating. J. Assist. Reprod. Genet. 30 (7), 953–961. https://doi.org/10.1007/S10815-013-0042-X.

Yang, H., Qiu, Y., Zeng, X., Ding, Y., Zeng, J., Lu, K., Li, D., 2016. Effect of a feeder layer composed of mouse embryonic and human foreskin fibroblasts on the proliferation of human embryonic stem cells. Exp. Ther. Med. 11 (6), 2321–2328. https://doi.org/10.3892/ETM.2016.3204/HTML.

Yu, L., Wei, Y., Duan, J., Schmitz, D.A., Sakurai, M., Wang, L., Wu, J., 2021a. Blastocyst-like structures generated from human pluripotent stem cells. Nature 591 (7851), 620–626. https://doi.org/10.1038/S41586-021-03356-Y.

Yu, L., Wei, Y., Sun, H.X., Mahdi, A.K., Pinzon Arteaga, C.A., Sakurai, M., Wu, J., 2021b. Derivation of intermediate pluripotent stem cells amenable to primordial germ cell specification. Cell Stem Cell 28 (3), 550–567.e12. https://doi.org/10.1016/J.STEM.2020.11.003.

Zdravkovic, T., Nazor, K.L., Larocque, N., Gormley, M., Donne, M., Hunkapillar, N., Fisher, S.J., 2015. Human stem cells from single blastomeres reveal pathways of embryonic or trophoblast fate specification. Development 142 (23), 4010–4025. https://doi.org/10.1242/DEV.122846/-/DC1.

Zhou, W., Choi, M., Margineantu, D., Margaretha, L., Hesson, J., Cavanaugh, C., Ruohola-Baker, H., 2012. HIF1α induced switch from bivalent to exclusively glycolytic metabolism during ESC-to-EpiSC/hESC transition. EMBO J. 31 (9), 2103–2116. https://doi.org/10.1038/emboj.2012.71.

Zhou, J., Hu, J., Wang, Y., Gao, S., 2023. Induction and application of human naive pluripotency. Cell Rep. 42 (4), 112379 https://doi.org/10.1016/J.CELREP.2023.112379.